

The pressure drop along rectangular microchannels containing bubbles†

Michael J. Fuerstman,^a Ann Lai,^a Meghan E. Thurlow,^a Sergey S. Shevkoplyas,^a Howard A. Stone^{*b} and George M. Whitesides^{*a}

Received 1st May 2007, Accepted 24th July 2007

First published as an Advance Article on the web 22nd August 2007

DOI: 10.1039/b706549c

This paper derives the difference in pressure between the beginning and the end of a rectangular microchannel through which a flowing liquid (water, with or without surfactant, and mixtures of water and glycerol) carries bubbles that contact all four walls of the channel. It uses an indirect method to derive the pressure in the channel. The pressure drop depends predominantly on the number of bubbles in the channel at both low and high concentrations of surfactant. At intermediate concentrations of surfactant, if the channel contains bubbles (of the same or different lengths), the total, aggregated length of the bubbles in the channel is the dominant contributor to the pressure drop. The difference between these two cases stems from increased flow of liquid through the “gutters”—the regions of the system bounded by the curved body of the bubble and the corners of the channel—in the presence of intermediate concentrations of surfactant. This paper presents a systematic and quantitative investigation of the influence of surfactants on the flow of fluids in microchannels containing bubbles. It derives the contributions to the overall pressure drop from three regions of the channel: (i) the slugs of liquid between the bubbles (and separated from the bubbles), in which liquid flows as though no bubbles were present; (ii) the gutters along the corners of the microchannels; and (iii) the curved caps at the ends of the bubble.

I. Introduction

We have developed a simple experimental method to compare the numbers, lengths and speeds of gas bubbles moving in two parallel microfluidic channels; we use this method to determine the effect of the bubbles on the pressure drop between two positions in a microchannel of rectangular cross-section. We consider systems in which the bubbles move through aqueous solutions, both with and without surfactant. By developing a model for the fluid–dynamical response, we indirectly determine the dependence of the pressure drop along the channel—for a fixed rate of flow of liquid—on five parameters: (i) the number of bubbles in the channel; (ii) the total length of the bubbles in the channel; (iii) the aspect ratio of the channel, defined as the ratio of the height of the channel to its width; (iv) the concentration of surfactant (either Tween-20 or sodium dodecyl sulfate, SDS) in the bulk solution; and (v) the viscosity of the liquid in the channel. Predicting the paths that bubbles will take through microfluidic networks—and therefore developing the capability to route bubbles through microfluidic systems without the use of external valves or switches—requires a thorough understanding of the contributions of these parameters to the pressure drop along channels with bubbles. We determined experimentally that when the concentration of surfactant in the liquid was ≤ 0.1 [CMC]

([CMC] is the critical micelle concentration), the pressure drop along the channel depended primarily on the number of bubbles in the channel. When the concentration of surfactant was 1000 [CMC] (for Tween-20) or 10 [CMC] (for SDS) the pressure drop also depended chiefly on the *number* of bubbles. At intermediate concentrations of surfactant, however, the total *length* of the bubbles in the channel was the dominant contributor. We also determined that the bubble and liquid move at approximately the same speeds when there is no surfactant in the liquid—a behavior similar to that observed previously in systems containing bubbles moving through cylindrical tubes^{1–4}—while, at intermediate concentrations of surfactant, the liquid moves approximately twice as fast as the bubble—a behavior *not* observed in analogous experiments in a cylindrical tube.

The ability to predict how a bubble or droplet^{5–7} will move through a microfluidic device, in the presence or absence of surfactant, is important for a number of current and emerging applications in which bubbles are used to enhance mixing,^{8–10} to facilitate chemical reactions,^{11,12} or to serve as tools for logic-based computations.¹³ As microfluidic devices grow in complexity, the number of possible paths that bubbles can take through the devices will grow to accommodate parallel processes or multiple functionalities that employ multiple bubbles on one chip. To design microfluidic networks that do not require valves or switches to route bubbles from one region of a device to the next, one must be able to predict the paths of the bubbles through the network.¹⁴ Understanding how the pressure drop along a channel depends on the number and lengths of the bubbles that move through it is crucial to making these kinds of predictions.

^aDepartment of Chemistry and Chemical Biology, Harvard University, Cambridge, Massachusetts 02138, USA.

E-mail: gwhitesides@gmwgroup.harvard.edu

^bSchool of Engineering and Applied Sciences, Harvard University, Cambridge, Massachusetts 02138, USA. E-mail: has@seas.harvard.edu

† Electronic supplementary information (ESI) available: Fabrication of the device and design of the microfluidic network. See DOI: 10.1039/b706549c

We focused on systems that were characterized by low capillary number (Ca). The capillary number is a measure of the importance of viscous to interfacial forces; $Ca \equiv \mu V/\gamma$, where μ ($\text{kg m}^{-1} \text{s}^{-1}$) is the viscosity of the liquid phase, V (m s^{-1}) is the linear velocity of the fluid, and γ (kg s^{-2}) is the interfacial energy between the gas and the liquid. In our experiments, Ca was on the order of 10^{-3} . The end-caps of the bubbles have nearly constant radii of curvature at values of Ca that are this low. Theoretical and modeling results for the pressure drop along microchannels containing bubbles are available within this range of Ca .^{15,16} The bubbles that we measured were longer than the width of the channel and were hydrodynamically isolated—that is, they were separated from each other by a distance greater than the height of the channel—because lab-on-a-chip devices that employ bubbles most frequently use such long, isolated bubbles.^{9,12} The pressure drop added by isolated bubbles surrounded by a liquid that contains surfactant, and moving at speeds typical of those in microfluidic devices, has not previously been investigated experimentally for channels of rectangular cross-section; rectangular channels are the common configuration for most microfluidic channels made using photolithographic or soft-lithographic methods. Ratulowski and Chang, Stebe *et al.*, and Park have examined the effect of surfactant on the pressure drop due to bubbles in cylindrical channels.^{17–19} Other groups have measured the pressure drop due to bubbles that were smaller than the width of the channel² or were non-isolated.^{2,20,21} Adzima and Velankar,²² for example, used external pressure gauges to measure the pressure drop along a channel that contained droplets of water moving in a continuous stream of hexadecane. We determine the influence of the numbers and lengths of bubbles on the pressure drop along a microchannel in the presence and absence of surfactants without using pressure sensors.

Instead of measuring the difference in pressure directly in the microfluidic system, we inferred the pressure drop by measuring the lengths, speeds and number of bubbles that moved through two parallel channels using a CCD camera attached to a microscope, and fitting these parameters to an equation based on a hydrodynamic model of the pressure drop along the channel. Unlike previous experimental studies, this method allowed us to differentiate between the dependence of the overall pressure drop on the lengths and numbers of bubbles in the channel, and to determine the contributions of different parts of the bubble/liquid system to the overall pressure drop along the channel. This method also allowed us to determine the influence of surfactants on the motion of bubbles and liquid through channels of rectangular cross-section.

II. The pressure drop along a microchannel containing bubbles

A. The flow of liquid through a microchannel

The flow of liquids through microfluidic channels usually occurs at low Reynolds numbers (Re). A measure of the relative importance of inertial to viscous forces, $Re \equiv \rho VL/\mu$, where ρ (kg m^{-3}) is the density of the liquid, L (m) is a characteristic length of the system, in this case the height of the

channels, μ is the viscosity of the liquid ($\text{kg m}^{-1} \text{s}^{-1}$), and V (m s^{-1}) is the linear velocity of liquid through the channels. In our experiments, Re was on the order of 0.1 to 1. For systems at low Re , eqn (1) relates Q ($\text{m}^3 \text{s}^{-1}$), the volumetric rate of flow of liquid between two points in a channel, and ΔP ($\text{kg m}^{-1} \text{s}^{-2}$), the difference in pressure between those two points. These two terms are proportional; the constant of proportionality is called the fluidic resistance, R ($\text{kg m}^{-4} \text{s}^{-1}$), of the segment of the channel that is bounded by the two points.

$$\Delta P = QR \quad (1)$$

In a rectangular channel in which there are no bubbles or obstructions present, the laminar flow of a single liquid phase through the channel approximately follows eqn (2), where L (m) is the length of the channel, W (m) is the width of the channel, H (m) is the height of the channel, and a is a dimensionless parameter that depends on aspect ratio, W/H , and is defined in eqn (3).²³

$$\Delta P = \frac{a\mu QL}{WH^3} \quad (2)$$

$$a = 12 \left[1 - \frac{192H}{\pi^5 W} \tanh\left(\frac{\pi W}{2H}\right) \right]^{-1} \quad (3)$$

Eqn (2) is accurate to within 0.26% for any rectangular channel that has $W/H < 1$, provided that the Reynolds number (Re) is below ~ 1000 .²³ Eqn (2) is independent of the presence or absence of surfactant for the range of surfactant concentrations studied here (other than for a possible change in the viscosity of the liquid due to the surfactant; this change is negligible in our experiments).

B. The pressure drop along a channel that contains bubbles

The flow of liquid through a microchannel that contains bubbles is more complicated than the flow of a single phase through a channel. To construct an expression for the pressure drop along such a channel, we characterize the hydrodynamic response of three types of regions (see Fig. 1): (i) the parts of the channel in which the liquid flows and no bubbles are present, denoted by the subscript “nb”; (ii) the regions of the central section, or the body, of the bubbles (the part of the bubbles between the end-caps); and (iii) the region of the end-caps of the bubbles.^{15,16,24,25} Eqn (4) relates the total pressure drop along the channel, ΔP_{Total} , to the pressure drops across these three regions, where ΔP_{nb} is the total pressure drop across the regions in which liquid flows with no bubbles present, ΔP_{body} is the pressure drop across the regions of the bodies of the bubbles, and ΔP_{caps} is the pressure drop across the regions containing the caps of the bubbles (the units of the three ΔP terms are $\text{kg m}^{-1} \text{s}^{-2}$):

$$\Delta P_{\text{Total}} = \Delta P_{\text{nb}} + \Delta P_{\text{body}} + \Delta P_{\text{caps}} \quad (4)$$

Fig. 1A shows a schematic diagram of the partitioning of ΔP_{Total} . Since Re is small (< 1), the pressure drop across all of the transitional zones between the three regions is negligible.

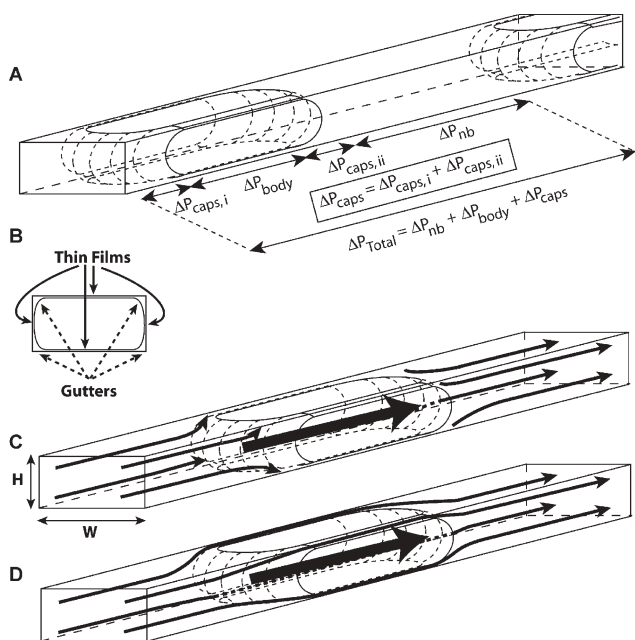


Fig. 1 (A) Partitioning the pressure drop along a microchannel containing a bubble into components. The total overall pressure drop, ΔP_{Total} , is equal to the sum of the pressure drops across the caps of the bubble, ΔP_{caps} , the pressure drop across the body of the bubble, ΔP_{body} , and the pressure drop across the region of the channel that does not contain a bubble, ΔP_{nb} . (B) A schematic view of the bubble down the long axis of the channel. The thin films are in between the flat sections of the bubble and the walls of the channel, while the gutters run down the length of the bubble in the corners of the channel. (C) A schematic diagram in which the liquid does not flow past the bubble through the gutters. As it approaches the curved cap of the bubble, the liquid veers towards the walls of the channel, where it slows down. (D) A schematic diagram of the flow through a channel in which liquid flows past the bubble through the gutters. Since Ca is on the order of 10^{-3} in our experiments, we expect the shape of the bubbles to be similar for both plug flow (C) and corner flow (D) cases.

Eqn (5) relates ΔP_{nb} to Q_{nb} , the volumetric rate of flow of liquid through the parts of the channel in which the liquid flows and no bubbles are present. The term L_{nb} is the sum of the lengths of all of the parts of the channel in which bubbles are absent. The other parameters (W , H and μ) are defined as in eqn (2). We let V_{nb} (m s^{-1}) denote the average linear velocity of the liquid in the region where the liquid flows in the absence of bubbles. Since $Q_{\text{nb}} \equiv V_{\text{nb}}WH$, we can rewrite eqn (5) as eqn (6). Eqn (7) is an expression for L_{nb} —the length of the channel through which the liquid flows and where bubbles are absent—written in terms of quantities that we measured, where L_{Total} (m) is the length of the channel along which ΔP_{Total} is applied and $L_{\text{cap-to-cap}}$ (m) is the total length of the bubble—measured from the tip of the front cap of each bubble to the tip of the back cap—of all of the bubbles in the branch. Substituting eqn (7) into eqn (6) yields eqn (8).

$$\Delta P_{\text{nb}} = \frac{a\mu Q_{\text{nb}} L_{\text{nb}}}{WH^3} \quad (5)$$

$$\Delta P_{\text{nb}} = \frac{a\mu V_{\text{nb}} L_{\text{nb}}}{H^2} \quad (6)$$

$$L_{\text{nb}} = L_{\text{Total}} - L_{\text{cap-to-cap}} \quad (7)$$

$$\Delta P_{\text{nb}} = \frac{a\mu V_{\text{nb}} (L_{\text{Total}} - L_{\text{cap-to-cap}})}{H^2} \quad (8)$$

The body, or the region between the end-caps of the bubbles, includes the gaseous bubble itself, four gutters (the areas bounded by the curved body of the bubble and the corners of the channel), and four thin films of liquid between the flat surfaces of the bubble and the walls of the channel (Fig. 1A). Since the pressure is uniform everywhere inside the bubble, ΔP_{body} describes the pressure drop in the liquid along the length of the body. The gutters and the thin films all run from one end-cap of a bubble to the other; the pressure drops along each of the gutters and thin films equal ΔP_{body} . We chose to construct an expression for the pressure drop along a gutter rather than a thin film, since liquid preferentially flows through the gutters rather than through the much narrower thin films at the sides of the channels. We base this assumption that the contribution to pressure drop across the bubble due to the thin films is negligible in the presence of gutters on the work of Ransohoff and Radke.²⁴ Since these flows have low Re , we assume that the pressure drop along a gutter has a form similar to eqn (5). Eqn (9) linearly relates ΔP_{body} to Q_{gutter} , the volumetric rate of flow through one gutter. For the sake of simplicity, we chose H as the scale for length that is relevant to the flow of liquid through the gutter. In eqn (9), L_{body} is the total length of the bodies of the bubbles in the channel and b' is a dimensionless parameter that depends on the ratio of the characteristic length of the gutters to the selected scale for length, H . We were unable to determine the explicit analytical form of b' experimentally. Fig. 1B and 1C show schematic diagrams of the paths that the liquid follows when it flows (or does not flow) through the gutters.

$$\Delta P_{\text{body}} = \frac{b'\mu Q_{\text{gutter}} L_{\text{body}}}{H^4} \quad (9)$$

We were unable to measure, either directly or indirectly, Q_{gutter} in eqn (9). We therefore rewrite the equation in terms of quantities we could measure and dimensionless parameters that we could vary to obtain an estimate by empirical fitting. We define $Q_{\text{gutter}} \equiv dV_{\text{nb}}H^2$ where d is a dimensionless parameter that depends on the ratio of the characteristic length for the gutters to the selected scale for length, H and on the ratio of V_{gutter} to V_{nb} . We then rewrite eqn (9), the expression for ΔP_{body} , to obtain eqn (10).

$$\Delta P_{\text{body}} = \frac{b\mu V_{\text{nb}} L_{\text{body}}}{H^2}, \quad b \equiv b'd \quad (10)$$

Bretherton derived an expression for ΔP_{caps} for a bubble in a channel of circular cross-section in the absence of surfactant; this pressure drop results from the dissipation in the transitional regions between the hemispherical end caps of the bubble and the thin film along the body of the bubble.¹ Wong *et al.* extended Bretherton's analysis to channels of rectangular cross-section with the aid of numerical computation.^{15,16} Both groups found that ΔP_{caps} scales as γ/R , where R is the radius of the cross-section of a circular tube. γ/R is

proportional to $Ca^{2/3}$. Ca , the capillary number, is now defined as $\mu V_{nb}/\gamma$, where γ is the interfacial energy between the liquid outside the bubble and the gas inside of it (kg s^{-2}), μ is the viscosity of the liquid ($\text{kg m}^{-1} \text{s}^{-1}$), and V_{nb} is the speed of the liquid (m s^{-1}). Other groups verified this result experimentally for bubbles in cylindrical channels.^{17,26} In a microchannel with a rectangular cross-section, we chose H as the scale for length to replace R . Eqn (11) gives the expression for ΔP_{caps} , where n is the number of bubbles in the channel. The analysis and computations by Wong *et al.* do not provide an explicit functional form for c , which is a dimensionless parameter dependent on H/W , and which relates the characteristic length for the end-cap region to the selected scale for length, H .

$$\Delta P_{\text{caps}} = \frac{cn\gamma Ca^{2/3}}{H} = \frac{cnV_{nb}\mu Ca^{-1/3}}{H} \quad (11)$$

Substituting eqn (8), (10) and (11) into eqn (4) gives eqn (12), which describes the total pressure drop along a channel that contains bubbles and simplifies to eqn (13).

$$\begin{aligned} \Delta P_{\text{Total,Model}} &= \Delta P_{\text{nb}} + \Delta P_{\text{body}} + \Delta P_{\text{caps}} \\ &= \frac{aV_{nb}\mu(L_{\text{Total}} - L_{\text{cap-to-cap}})}{H^2} + \\ &\quad \frac{bV_{nb}\mu L_{\text{body}}}{H^2} + \frac{cnV_{nb}\mu HCa^{-1/3}}{H^2} \end{aligned} \quad (12)$$

$$\Delta P_{\text{Total,Model}} = \frac{V_{nb}\mu}{H^2} [a(L_{\text{Total}} - L_{\text{cap-to-cap}}) + bL_{\text{body}} + cnHCa^{-1/3}] \quad (13)$$

In our experiments, we typically measured V_b , the linear velocity of the bubble (m s^{-1}), rather than V_{nb} , because we were able to obtain V_b directly for each experiment by measuring how far a bubble moved in a given period of time. To rewrite eqn (13) only in terms of quantities we measured and dimensionless parameters that we could vary to obtain an estimate by empirical fitting, we define $V_{nb} \equiv \alpha V_b$, where α is a dimensionless parameter relating V_{nb} to V_b (which we determined experimentally). By applying this definition to eqn (13), we obtain eqn (14), which is the most general form of our model for the pressure drop along a channel that contains bubbles.

$$\Delta P_{\text{Total,Model}} = \frac{\alpha V_b \mu}{H^2} [a(L_{\text{Total}} - L_{\text{cap-to-cap}}) + bL_{\text{body}} + cnH\alpha^{1/3}Ca^{-1/3}] \quad (14)$$

III. The experimental design

We produced the microfluidic devices using standard photolithographic and soft-lithographic techniques. We sealed a slab of polydimethylsiloxane (PDMS) that contained the channels to a flat slab of PDMS after exposing both pieces to an oxygen plasma for 60 s.²⁷ Fig. 2A is a schematic diagram of the microfluidic network that we used to make the bubbles. We used a syringe pump to introduce liquid into the system; the use of the syringe pump (in the absence of leaks) assures a

constant volumetric rate of flow of liquid through the system. The liquid and gas (nitrogen) flowed through separate inlets, which comprised an array of square posts that filtered debris

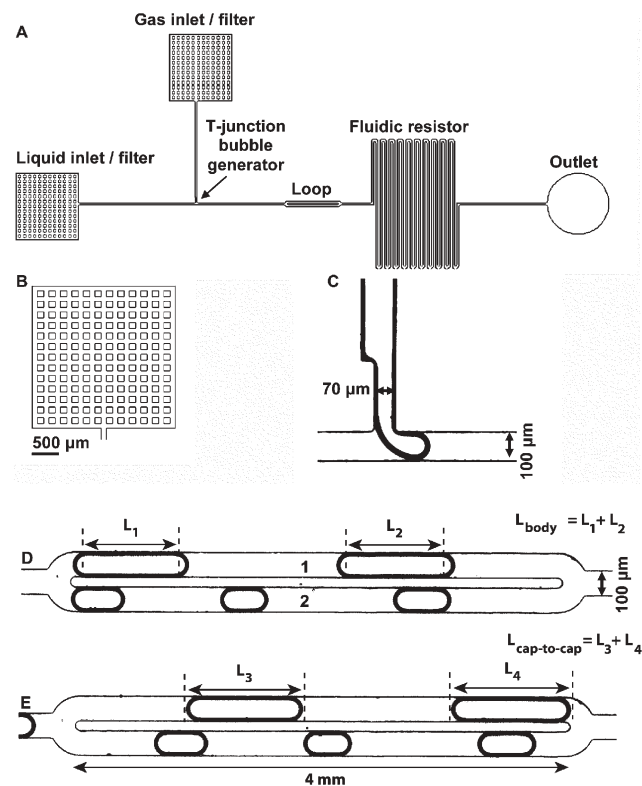


Fig. 2 (A) A schematic diagram of the microfluidic system that we used. The gas flowed initially through square inlets, which also served as filters to remove particulates from the flows. After forming at a T-junction intersection where the stream of liquid squeezed off bubbles with the advancement of the gaseous thread, the bubbles entered a region where the channel split into two identical branches, which combined farther downstream to form a loop. At the fork, depending on the magnitude of Ca and the initial length of the bubble, the bubble either remained intact or split into two daughter bubbles, the sizes of which are dependent on the resistance of the two branches relative to each other. We measured the lengths, numbers, and speeds of the bubbles in the two branches using a CCD camera. The bubbles then passed through a serpentine fluidic resistor and out of the device. (B) A close-up schematic diagram of the filters that formed the inlets of the device. (C) An optical micrograph of the gaseous thread advancing into the stream of liquid in a T-junction bubble-generator. The width of the channel carrying the gas into the T-junction was smaller than the width of the main channel carrying the liquid, to facilitate the pinching off of the neck of the gaseous thread that created the bubbles. The width of the channel carrying the gas decreased asymmetrically because it was easiest to design the channels in this manner. (D), (E) Optical micrographs of bubbles moving through the branches. The numbers (1 and 2) in (D) identify the two branches, each of which was $100 \mu\text{m}$ wide. The straight sections of the branches were 4 mm in length. These two micrographs mark the first and last frames in one of the video clips—in which the bubbles moved from left to right—that we analyzed to obtain data. The micrograph in (D) is marked to denote that the value of L_{body} in the top branch is defined to be equal to the sum of L_1 and L_2 . The micrograph in (E) is marked to denote that the value of $L_{\text{cap-to-cap}}$ in the top branch is defined to be equal to the sum of L_3 and L_4 .

out of the fluids (Fig. 2B), and met at a T-junction (Fig. 2C).²⁸ The stream of liquid squeezed off bubbles as the gaseous thread advanced into the main channel of the device.^{29,30} The exposure to the oxygen plasma rendered the walls of the channel hydrophilic, so that the liquid wet the walls while the gas phase did not. It is difficult to produce bubbles when the channels are hydrophobic because the gaseous thread sticks to the walls of the channel instead of pinching off to form bubbles. Moreover, the hydrophilic boundaries are necessary for these experiments since the model of section II is only valid if a thin film of liquid always separates the gas in the bubbles from the walls of the channel. In hydrophobic channels, the thin film often breaks; the gas then wets the walls of the channel and the bubbles slow as they move through the network.

We used rectangular channels that ranged in height from 20 to 75 microns, and in width from 68 to 132 microns. We used a profilometer to measure the height of the channels. We performed most of our experiments using channels that were 34–36 microns tall and 100 microns wide. Hence, the typical aspect ratio was $H/W \approx 0.35$.

We used four different kinds of solutions as the liquid phase: (i) pure water (electrical resistance of 18 M Ω , MilliQ water system, Millipore); (ii) aqueous solutions of Tween-20; (iii) aqueous solutions of sodium dodecyl sulfate (SDS); and (iv) aqueous solutions of glycerol. The surfactant Tween-20 (polyoxyethylene (20) sorbitan monolaurate) is non-ionic and has a molecular weight of 1228 g mol⁻¹ and a CMC of 0.059 mM. The second surfactant we used, SDS, is anionic, and has a molecular weight of 288 g mol⁻¹ and a CMC of 8.2 mM. We chose these two surfactants because one is charged and one non-ionic, and they are representative of typical chemical additives in lab-on-a-chip applications. We used glycerol to modify the viscosity of the water, so that we could test the influence of viscosity on the hydrodynamics of this multiphase system. The ESI† details experiments, using the pendant drop method, that we carried out to determine the interfacial tension of the solutions. These values were necessary to compute the capillary number, Ca .

A fluidic resistor (a long, serpentine channel) placed at the end of the network increased the pressure that we had to apply to the gas to create a bubble.²⁹ Eqn (2) shows that, for a fixed rate of flow of liquid, the pressure drop between two points in a channel depends on the distance between them. Without the resistor, the pressure required to create bubbles was too small (<1 psi) for our pressure regulator to operate in a controllable manner.

After forming at the T-junction, the bubbles moved down the channel to a fork, where the main channel split into two branches that recombined downstream to form a loop. The branches were mirror-images of one another: they had indistinguishable widths, heights and lengths. Fig. 2D shows an optical micrograph of bubbles moving through the two branches (labeled 1 and 2) of the loop. As the bubbles entered the fork, they either split into two bubbles or remained intact, depending on the magnitude of Ca and the initial length of the bubble.³¹

We captured movies of the bubbles moving left to right through the branches using a CCD camera, and cut the movies

into clips using Adobe Premiere. We selected only the clips where the liquid formed a continuous film between the bubble and the walls of the microchannels. We only used clips that were longer than 15 frames. Clips that were shorter than that length increased the experimental uncertainty too significantly, since the uncertainty in the speed of the bubble was inversely proportional to the length of the clip. Each clip depicted bubbles moving through the branches, with no bubbles entering or exiting the branches during the clip. Fig. 2D and 2E show the first and last still frames from one clip; the same bubbles that are in the branches in the image in Fig. 2D are also in the branches in Fig. 2E.

An in-house Matlab algorithm analyzed the individual clips to obtain (i) the length of the body of each bubble, *i.e.*, the part of a bubble between the caps, in each branch (Fig. 2D); (ii) the total length of each bubble, from the end of the front cap to the end of the back cap (Fig. 2E); (iii) the speeds at which each bubble moved; and (iv) the number of bubbles, n , in each branch. Fig. 2D shows that L_{body} is defined to be the sum of all of the lengths of the bodies of the bubbles in a branch, while Fig. 2E shows that $L_{\text{cap-to-cap}}$ is defined to be the sum of the length of all of the bubbles in a branch.

The branches were either 2 or 4 mm long. Obtaining precise values for the non-dimensional parameters in the hydrodynamic model (Section II) required that we capture video clips in which the difference in the number of bubbles in the two branches was as large as possible. Branches that were shorter than 2 mm typically failed to produce experiments in which the difference between the number of bubbles was greater than 1, since no more than two bubbles—which were usually between 0.3 and 1 mm long—could fit into a branch of that length and still yield a video clip that was at least 15 frames long. We did not use a clip if it depicted a bubble that was either shorter than the width of the channel—because the bubble then was unable to form gutters with the corners of the microchannel—or longer than 15 times the width of the channel—because the bubble was then prone to Rayleigh instabilities, which created waves on the surface of the bubble and caused the behavior of the system to deviate from the model.

We recorded the bubbles as they moved through two branches, rather than through one straight channel, because the pressure drops along both branches are always equal (this situation is analogous to the voltage drop being the same across two resistors connected in parallel in an electronic circuit). Since the cross-sectional geometries of the two branches are identical, we can assume that a , b , and c are the same for both branches. We can then rewrite eqn (14) to equate the pressure drops along the two branches.

$$\alpha_1 V_{\text{nb},1} [a(L_{\text{Total}} - L_{\text{cap-to-cap},1}) + bL_{\text{body},1} + c n_1 H \alpha_1^{1/3} Ca_1^{-1/3}] = \alpha_2 V_{\text{nb},2} [a(L_{\text{Total}} - L_{\text{cap-to-cap},2}) + bL_{\text{body},2} + c n_2 H \alpha_2^{1/3} Ca_2^{-1/3}] \quad (15)$$

To determine the values for b and c , we substituted the data that we obtained from our experiments into eqn (15) and varied these dimensionless parameters so that, when we plotted the two sides of the equations against one another, we obtained the least-squares best-fit line. We defined the confidence interval for the values of b and c as the range that

yielded coefficients of determination (R^2) that were greater than or equal to 0.985 (this value corresponds to 1.5% error, which we calculated to be characteristic of these systems) unless otherwise indicated.

IV. Results and discussion

A. The speed of the bubble versus the speed of the liquid

To determine the value of α for different concentrations of surfactant, we compared the speeds of a bubble moving through a branch to the speed of the fluid flowing through that branch. To ensure that the fluid flows with equal velocity through both branches, we selected only the clips where two bubbles of equal lengths are moving at the same time through both branches. We carefully checked the inlets of the device for leaks, and waited ten minutes after changing the rate of flow to obtain each point of data. We divided the rate of flow at which the pump operated by two to obtain the rate of flow through a single branch, since half of the flow went through each of the two branches. We calculated the average speed of the liquid in a branch by dividing the volumetric rate of flow through that branch by the cross-sectional area of that branch. As Fig. 3 shows, in the absence of surfactant, the speed of a bubble was, on average, within $5.4 \pm 3.7\%$ of the speed of the liquid. This result is consistent with the theoretical prediction of Wong *et al.*, for bubbles in channels of rectangular cross-section.¹⁶

When we used a 5.9 mM solution (100 [CMC]) of Tween-20 as the liquid phase, we found that, independent of V_{nb} and V_b , the liquid moved through the channel 2.1 times more rapidly than the bubble. Under these conditions, therefore, $\alpha = 2.1$, and the liquid flowed through the gutters and past the bubble. To visualize the flow in more detail for this case, we performed experiments with a 5.9 mM solution of Tween-20, in which 1 micron diameter latex particles were suspended. Fig. 3B–D show optical micrographs of the trajectory of a piece of debris that serves as a convenient tracer. The debris moved through a gutter from behind the tail of the bubble to a position in front of the head of the bubble. These figures demonstrate that liquid flows past the bubble.

For a 59 mM solution of Tween-20, we found that the liquid moved only 1.2 times faster than the bubbles, independent of V_{nb} and V_b , thus $\alpha = 1.2$ (Fig. 3). This result suggests that the flow through the gutters at 59 mM Tween-20 was slower than when the concentration of surfactant was 5.9 mM. We confirm this result using the model later in the paper. These results are significantly different from those from comparable experiments for systems with surfactant in cylindrical tubes^{17,18} and from theoretical predictions of the behavior of bubbles in systems without surfactant in rectangular channels.¹⁶ Wong *et al.*¹⁶ suggested a similar phenomenon—called “corner flow”—which only occurs at extremely low capillary numbers, $O(Ca) < 10^{-6}$. In our experiments, Ca is approximately 10^{-3} , which is several orders of magnitude larger than that in Wong *et al.*; this fact suggests that we observed a different phenomenon. In addition, their prediction did not lead to a large difference between the speed of the bubble and the speed of the liquid bypassing the bubble while, in our experiments, we observed a marked difference—larger than $O(Ca)$.

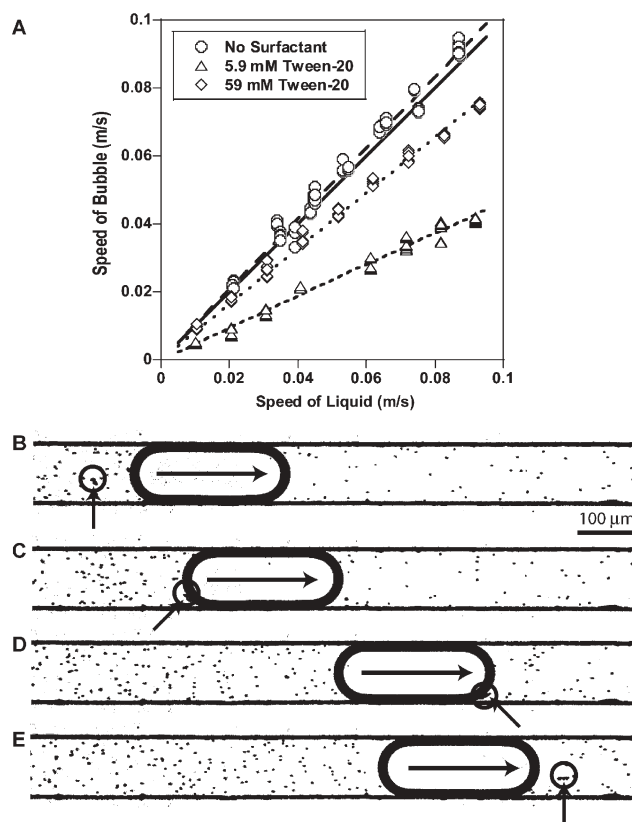


Fig. 3 (A) A plot of the speed of the bubbles moving through the system versus the speed of the liquid. In a system in which no surfactant was present (circles) the bubbles moved 4% faster than the average speed of the liquid. In the presence of 5.9 mM Tween-20 (triangles), the bubbles moved only half as rapidly through the channels as the liquid. At 59 mM Tween-20 (diamonds), the bubble moved at approximately 80% of the speed of the liquid. The solid line passes through the origin and has a slope equal to 1. The line marked by the longer dashes is a best-fit line, which is constrained to pass through the origin, for the data represented by the circles. The line marked by the shorter dashes is a best-fit line with a slope of 1.2 for the data represented by the triangles and is constrained to pass through the origin. The dashed line is a best-fit line with a slope of 2.1 for the data represented by the diamonds and is also constrained to pass through the origin. (B)–(D) Optical micrograph of a bubble moving from left to right through a solution of Tween-20 at 100 [CMC]. The liquid contained latex tracer particles that were 1 micron in diameter. The arrow points to a piece of debris that was larger than the tracer particles. The debris was behind the bubble initially, then moved through a gutter between the bubble and the walls of the channel and emerged in front of the bubble. This movement clearly indicates that the liquid moves significantly more rapidly than the bubble.

B. The pressure drop along a channel containing bubbles and liquid with no surfactant

To verify that the number of bubbles, n , in a branch influenced the overall pressure drop along the branch when there was no surfactant in the liquid phase, we plotted the ratio $V_{b,2}/V_{b,1}$ versus the ratio $L_{cap-to-cap,2}/L_{cap-to-cap,1}$ (Fig. 4A). We systematically compared these data for different numbers of bubbles in each branch. The data in Fig. 4A only overlap for clips in which the numbers of bubbles in the two branches differed by the same amount. For example, the data marked with the

symbol + in Fig. 4A represent clips in which one bubble moved through branch 1 and one bubble moved through branch 2. These results overlap with the data indicated by circles, which represent clips in which two bubbles moved through branch 1 and two bubbles moved through branch 2. Neither set of data overlap with the results marked by diamonds, which represent clips in which two bubbles moved through branch 1 and one bubble moved through branch 2. The pressure drop along each branch thus depended on the number of bubbles moving in each branch, in addition to the lengths of the bubbles. This result coincides with previously observed results for systems where bubbles are moving through cylindrical capillaries.^{17,26}

We also observed that larger ratios of $L_{\text{cap-to-cap},2}$ to $L_{\text{cap-to-cap},1}$ led to larger ratios of $V_{b,2}$ to $V_{b,1}$, as shown in Fig. 4A. This result suggests that, when no surfactant was present in the system, for cases in which $n_1 = n_2$, the bubbles moved slightly more rapidly through the branch that contained a greater total length of bubbles than through the branch that contained a smaller total length of bubbles. This result suggests that b is small relative to c in the hydrodynamic model (eqn (14)).

To obtain best-fit values for b and c , we inserted the data that we obtained from experiments in which there was no

surfactant in the system into eqn (15), with $a = 15$ (according to eqn (4)). Fig. 4B shows the resulting linear fit, which has a slope of 0.99.

The values of the dimensionless parameters that optimized the clustering of points onto the best-fit line were $b = 1.3$ (with a confidence interval of 0 to 8.0) and $c = 12$ (with a confidence interval of 9.9 to 16). The value of ΔP_{nb} that we derive using the model is on the order of 10^2 – 10^3 Pa, the value of ΔP_{body} is on the order of 10^0 – 10^1 Pa, and the value of ΔP_{caps} is on the order of 10^2 Pa. The net contribution to the overall pressure drop along the channel from the regions of the channel without bubbles is at least as much as the contribution from the regions containing the caps of the bubble. However, the ΔP_{caps} per unit length is typically greater than the ΔP_{nb} per unit length. Each of these regions contributes 10 to 10^3 times more significantly to the pressure drop along the channel than does the body region.

C. The dependence of c on the aspect ratio of the channel

We investigated the dependence of c on the aspect ratio of the channel in the absence of surfactant. We found the best-fit values of c for the model for channels that were 34 or

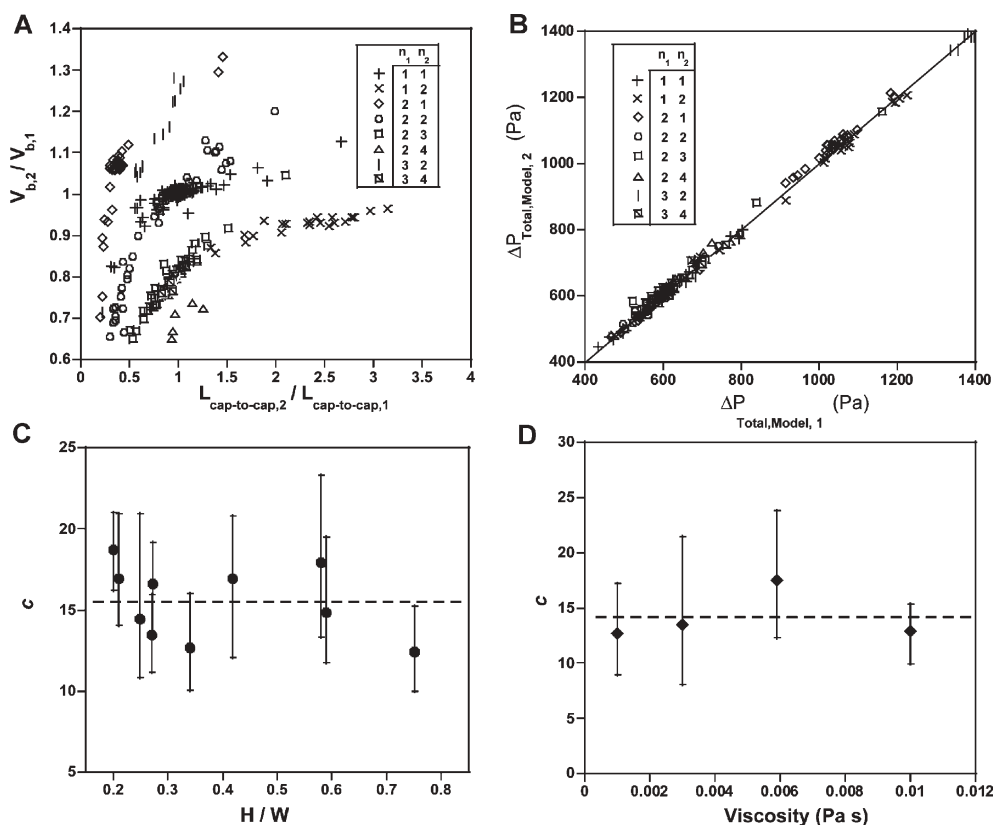


Fig. 4 (A) A plot of the ratio of the average velocities of bubbles in the two branches versus the ratio of the sum of the lengths of the bubbles in the two channels, for a system in which the continuous phase was water with no surfactant. The plot suggests that number of bubbles that moved through each branch affected the resistance that the bubbles added. (B) A plot of the pressure drop in branch 1, as expressed by the left-hand side of eqn (15), versus the pressure drop in branch 2, as expressed by the right-hand side of eqn (15). The best-fit line has a slope of 0.99. (C) A plot of the dimensionless parameter c as a function of the aspect ratio of the channel. The value of c is independent of the aspect ratio. The dashed line passes through the average value of the ten data. (D) A plot of the dimensionless constant c versus the viscosity of the aqueous glycerol solution comprising the continuous phase. The value of c is independent of the viscosity of the solution. The dashed line represents the average value of c for the four data points.

36 microns tall and 62, 86, and 132 microns wide, and systems that were 100 microns wide and 20, 21, 25, 27, 59 and 75 microns tall. The aspect ratios varied from 0.20 to 0.75. The term containing b —that is, the contribution to the pressure drop from the flow of liquid through the gutters—remained one or more orders of magnitude lower than the other two terms for all of the systems of varying aspect ratios, as detailed in the previous section. Fig. 4C shows that the value for c was independent of the aspect ratio of the channel, within experimental uncertainty. The dashed line represents the average of the ten values of c .

D. The dependence of c on the viscosity of the liquid

In order to test the influence of viscosity, and in particular to examine whether c was independent of viscosity as appears in the model in eqn (14), we obtained data for three systems in which the continuous liquid was an aqueous solution of glycerol: 35% glycerol by mass (viscosity, μ , of $0.0031 \text{ kg m}^{-1} \text{ s}^{-1}$), 52% ($0.0069 \text{ kg m}^{-1} \text{ s}^{-1}$) and 60% ($0.0108 \text{ kg m}^{-1} \text{ s}^{-1}$). Fig. 4D shows a plot of the values of c versus the viscosity of the liquid. The values of c for the experiments are all indistinguishable within the confidence intervals; the dashed line represents the average of the data. We determined confidence intervals for these values of c by adjusting that parameter until the R^2 value decreased to less than 0.975 (thus, we allowed for 2.5% uncertainty in the value of c). This uncertainty is greater than that of other systems that we examined because of the added experimental uncertainty in the values of the viscosity and of the interfacial tension of the continuous phases.

E. The pressure drop along a channel containing bubbles and liquid with Tween-20

We next added surfactant to the continuous liquid. We carried out experiments in which the concentration of Tween-20 in the water was 5.9 mM (100 times the CMC) to determine the contributions to the pressure drop along a branch in the presence of surfactants. To see whether the number of bubbles influenced the pressure drop along the branches, we plotted $V_{b,2}/V_{b,1}$ versus $L_{\text{cap-to-cap},2}/L_{\text{cap-to-cap},1}$ (Fig. 5A) in a manner similar to the case in which there was no surfactant in the water. Unlike the case in which no surfactant was present, all of the data collapse onto a single curve. This result suggests that the number of bubbles moving in a branch did not contribute to the pressure drop along the branch.

These experiments also differed from those in which there was no surfactant in the liquid in that bubbles moved *more slowly* through the branch in which L_{body} was greater (Fig. 4A). This result suggests that the contribution of the flow through the gutters to the overall pressure drop along the branches was not negligible, as it was in the case in which there was no surfactant in the liquid.

To determine values for b in the hydrodynamic model, and to determine the relative magnitudes of the contributions of the three terms to the overall pressure drop through the branches, we plotted the left-hand side of eqn (15) against the right-hand side, as shown in Fig. 5B. The best-fit line has a slope of 1. For a value of $a = 15$, we found that the best-fit

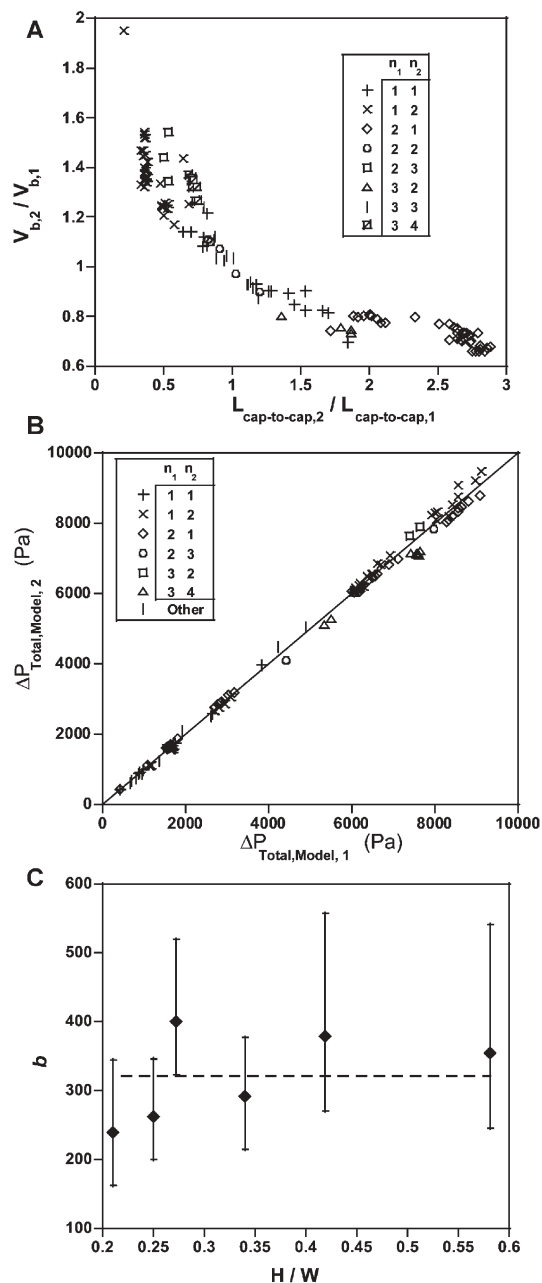


Fig. 5 (A) A plot of the ratio of the average velocity of the bubbles in branches 1 and 2 versus the ratio of the sum of the lengths of the bubbles in branches 1 and 2, for a system in which the concentration of Tween-20 was 100 [CMC]. This plot shows that this system behaved oppositely to one in which there was no surfactant—the number of bubbles in a branch *did not* influence the resistance of the branch. (B) A plot of the pressure drop in branch 1, as expressed by the left-hand side of eqn (15), versus the pressure drop in branch 2, as expressed by the right-hand side of eqn (15). The best-fit line has a slope of 1. (C) A plot of the dimensionless parameter b as a function of the aspect ratio of the channel. The value of b is independent of the aspect ratio. The dashed line passes through the average value of the six data points.

value of b was 96 (with a confidence interval of 130 to 170); we also verified that the best-fit value of c was zero. The ΔP_{body} per unit length is typically greater than the ΔP_{nb} per unit length by an order of magnitude.

F. The dependence of b on the aspect ratio of the channel with Tween-20

We determined that b is independent of the aspect ratio of the channel for systems in which the continuous phase was an aqueous solution of Tween-20 at 100 [CMC]. The plot in Fig. 5C shows this result. The dashed line represents the average of the six data. This result indicates that the pressure drop along the gutters of the bubble does not depend on the aspect ratio of the channel.

G. The dependence of the contributions of ΔP_{body} and ΔP_{caps} on the concentration of surfactant in the liquid

In order to determine how the relative contributions of ΔP_{body} and ΔP_{caps} to ΔP_{Total} varied with the concentration of surfactant in the liquid, we carried out experiments in which the aqueous continuous phase contained Tween-20 in concentrations of 0.00059 mM, 0.0059 mM, 0.59 mM, 5.9 mM and 59 mM (these values correspond to concentrations of 0.01, 0.1, 10, 100 and 1000 [CMC]). We also used the pendant drop method to obtain values for the surface tension of these solutions (see ESI†). Around the CMC, the thin film around the bubbles dewet the walls of the channel in a seemingly random fashion; when dewetting occurred, the gaseous bubbles contacted the wall directly and slowed, sometimes stopping completely in one of the branches. Our model does not account for this behavior, so we were unable to obtain reliable data for concentrations near the CMC for Tween-20. We did not observe this dewetting phenomenon with SDS.

As the concentration of surfactant increased, the value of c —and therefore the contribution of the caps of the bubble to the pressure drop along the channel—decreased from its value in pure water to zero at 0.59 mM Tween-20 (Fig. 6A). Conversely, the value of b —which represents the contribution of the flow of liquid through the gutters—increased from its value in pure water to a maximum of ~ 190 at 10 [CMC]. At 59 mM Tween-20 (1000 [CMC]), however, the value of b dropped to 48 (with a confidence interval from 43 to 82), while the value of c increased from zero to 35 (with a confidence interval from 17 to 68). This result suggests that the flow through the gutters slowed at high concentrations of Tween-20.

We also observed the same trends in the values of b and c with SDS (Fig. 6B) as we did with Tween-20. We carried out experiments in which the water contained 0.082 mM, 0.82 mM, 8.2 mM and 82 mM SDS (these values correspond to concentrations of 0.01, 0.1, 1 and 10 [CMC]). We extrapolated the values for the surface tensions of these solutions from trends reported by Shen *et al.*³² In the case of SDS, the range of concentrations of surfactant over which ΔP_{body} exceeded ΔP_{caps} —by approximately two orders of magnitude—was narrower than with Tween-20, for which ΔP_{body} was greater than ΔP_{caps} over three orders of magnitude.

The trends that we report in Fig. 6 are similar to those found by Stebe *et al.*¹⁸ They reported that the pressure drop across a bubble in a cylindrical channel increased relative to the pressure drop along a liquid-filled channel of the same dimensions when they added surfactant to the continuous liquid. They observed that—as they increased the concentration of

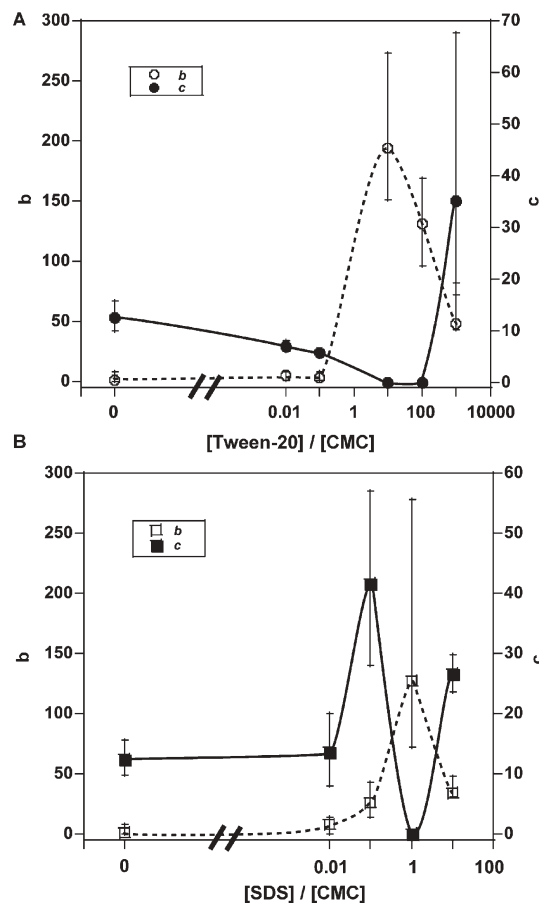


Fig. 6 (A) A plot of the dependence of b and c on the concentration of Tween-20 in the continuous phase (expressed as a multiple of the CMC, 59 μM). The value of b corresponds to the left axis and c corresponds to the right axis. The value of c decreases to zero and then increases again as the concentration increases. The value of b is close to zero when no surfactant is present; b increases to a maximum around 100 [CMC] and begins to decrease again as the concentration increases further. The lines are guides for the eyes. (B) A similar plot to (A) with SDS as the surfactant (CMC = 8.2 mM). The values of b and c follow the same trends as in the experiments with Tween-20.

surfactant above the CMC—the pressure drop across the bubble relative to the pressure drop across a plug of liquid of the same length decreased once more.

V. Conclusions

We used a hydrodynamic model and experiments to understand the motion of liquid and bubbles through rectangular microchannels in the presence and absence of Tween-20 and SDS. We established that the dominant contributor per unit length to the pressure drop along a microchannel of rectangular cross-section that contains bubbles is dependent on the concentration of surfactant present in the liquid in which the bubbles move. In the absence of surfactant, the pressure declines most rapidly in the region containing the end-caps (Fig. 7); hence, the number of bubbles in the channel influences the pressure drop most significantly. At intermediate concentrations of surfactant (within one or two orders of magnitude of the CMC), the pressure declines most rapidly

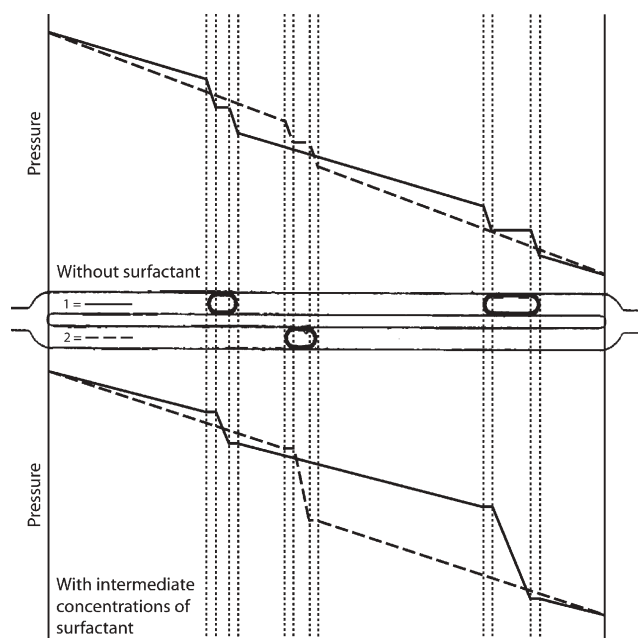


Fig. 7 A qualitative plot of the pressure along paired microchannels containing different numbers of bubbles. The overall pressure drop is the same for both microchannels. The top plot shows the drop in pressure along the microchannels for systems in the absence of surfactant. The pressure declines most rapidly in the regions containing the end-caps of the bubbles. The bottom plot shows the drop in pressure along the microchannels for systems containing intermediate levels of surfactant. For these cases, the pressure declines most rapidly across the body of the bubble.

across the body of the bubble (Fig. 7); therefore, the total length of the bubbles influences the pressure drop most significantly. At high concentrations of surfactant, the system effectively behaves as if there were no surfactant present in the liquid, and the pressure declines most rapidly in the regions containing the end-caps.

We believe that the contribution of the region containing the body of the bubble to the overall pressure drop depends on the flow of the liquid through the gutters. In the absence of surfactants, the flow of the liquid through the gutters is negligible, and the bubble moves at approximately the same speed as the liquid. At intermediate concentrations of surfactant, the liquid flows rapidly through the gutters of the channel. This flow allows the bubble to move with a speed significantly lower than the average speed of the liquid. This response deviates from previous experiments with bubbles in circular tubes. At higher concentrations of surfactant, however, the rate of flow through the gutter slows substantially. To the best of our knowledge, this paper is the first to report the concentration-dependent flow of liquid through the gutters around a bubble moving in a rectangular channel.

To describe this surfactant-mediated response, we propose a mechanism, which draws on previous studies on bubbles in cylindrical channels; these studies invoke gradients in the concentration of surfactant to explain changes in the pressure drop across bubbles in the presence and absence of surfactant.^{17,18} In this mechanism, the surfactant molecules at the interface between the liquid and the bubble in the gutters are

swept from the back toward the front of the bubble by the flow of liquid on the surface of the bubble. This flow creates a gradient in the concentration of surfactant along the body of the bubble, which in turn creates a gradient in the surface tension along the bubble. This gradient in the surface tension creates a pressure drop across the length of the bubble, resulting in flow through the gutters. At high concentrations of surfactant, however, molecules of Tween-20 or SDS adsorb onto the interface more rapidly than the flow of liquid on the surface of the bubble can establish a gradient. With this rapid remobilization, the saturated interface then behaves like a bubble in liquid with no surfactant, and liquid can no longer flow through the gutters.¹⁸

The findings that this paper details are important for multiphase fluidics, especially as they pertain to microchannels of rectangular cross-section—the geometry most compatible with standard photolithographic procedures. These results will facilitate the manipulation of bubbles in microfluidic devices, especially in systems where the bubbles that travel through the device do not have uniform size.

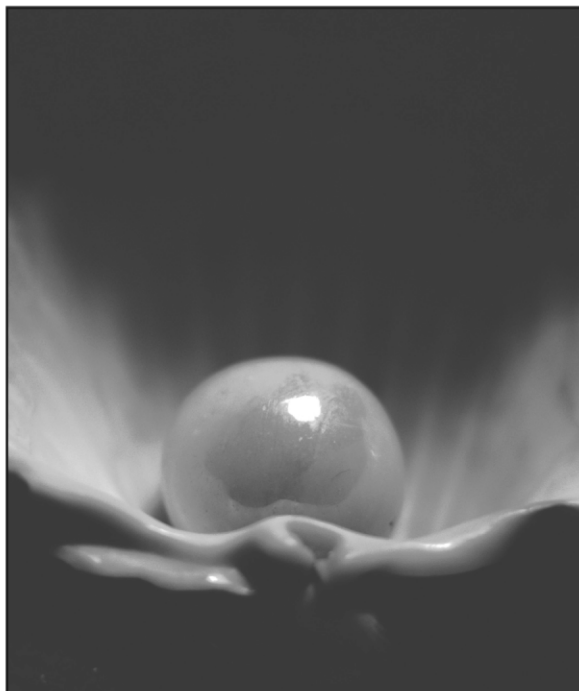
Acknowledgements

This work was supported by the U.S. Department of Energy under award DE-FG02-OOER45852. The Harvard Center for Nanoscale Systems (DMR-0213805) provided the microfabrication facilities and high-speed cameras. We thank Professor David Weitz, Dr Carlos Martinez, Andrew Utada and Anderson Shum for the use of and help with the pendant drop experiments and software.

References

- 1 F. P. Bretherton, *J. Fluid Mech.*, 1961, **10**, 166.
- 2 T. Cubaud and C.-M. Ho, *Phys. Fluids*, 2004, **16**, 4575.
- 3 W. B. Kolb and R. L. Cerro, *Phys. Fluids A*, 1993, **5**, 1549–1557.
- 4 W. B. Kolb and R. L. Cerro, *J. Colloid Interface Sci.*, 1993, **159**, 302–311.
- 5 W. Engl, M. Roche, A. Colin, P. Panizza and A. Ajdari, *Phys. Rev. Lett.*, 2005, **95**, 208304.
- 6 M. J. Fuerstman, P. Garstecki and G. M. Whitesides, *Science*, 2007, **315**, 828–832.
- 7 F. Jousse, R. Farr, D. R. Link, M. J. Fuerstman and P. Garstecki, *Phys. Rev. E*, 2006, **74**, 036311.
- 8 A. Gunther, M. Jhunjhunwala, M. Thalmann, M. A. Schmidt and K. F. Jensen, *Langmuir*, 2005, **21**, 1547–1555.
- 9 P. Garstecki, M. J. Fuerstman, M. A. Fischbach, S. K. Sia and G. M. Whitesides, *Lab Chip*, 2006, **6**, 207–212.
- 10 P. Garstecki, M. A. Fischbach and G. M. Whitesides, *Appl. Phys. Lett.*, 2005, **86**, 244108.
- 11 A. Gunther, S. A. Khan, M. Thalmann, F. Trachsel and K. F. Jensen, *Lab Chip*, 2004, **4**, 278–286.
- 12 S. A. Khan, A. Gunther, M. A. Schmidt and K. F. Jensen, *Langmuir*, 2004, **20**, 8604–8611.
- 13 M. Prakash and N. Gershenfeld, *Science*, 2007, **315**, 832–835.
- 14 G. Cristobal, J. P. Benoit, M. Joanicot and A. Ajdari, *Appl. Phys. Lett.*, 2006, **89**, 034104.
- 15 H. Wong, C. J. Radke and S. Morris, *J. Fluid Mech.*, 1995, **292**, 71–94.
- 16 H. Wong, C. J. Radke and S. Morris, *J. Fluid Mech.*, 1995, **292**, 95.
- 17 J. Ratulowski and H. C. Chang, *J. Fluid Mech.*, 1990, **210**, 303–328.
- 18 K. J. Stebe, S. Y. Lin and C. Maldarelli, *Phys. Fluids A*, 1991, **3**, 3–20.
- 19 C.-W. Park, *Phys. Fluids A*, 1992, **4**, 2335–2347.
- 20 N. D. Denkov, V. Subramanian, D. Gurovich and A. Lips, *Colloids Surf., A*, 2005, **263**, 129–145.

- 21 E. Terriac, J. Etrillard and I. Cantat, *Europhys. Lett.*, 2006, **74**, 909–915.
- 22 B. J. Adzima and S. S. Velankar, *J. Micromech. Microeng.*, 2006, **16**, 1504–1510.
- 23 C. J. Morris and F. K. Forster, *Exp. Fluids*, 2004, **36**, 928–937.
- 24 T. C. Ransohoff and C. J. Radke, *J. Colloid Interface Sci.*, 1988, **121**, 392–401.
- 25 A. L. Hazel and M. Heil, *J. Fluid Mech.*, 2002, **470**, 91–114.
- 26 M. T. Kreutzer, F. Kapteijn, J. A. Moulijn, C. R. Kleijn and J. J. Heiszwolf, *AIChE J.*, 2005, **51**, 2428–2440.
- 27 M. K. Chaudhury and G. M. Whitesides, *Langmuir*, 1991, **7**, 1013.
- 28 T. Thorsen, R. W. Roberts, F. H. Arnold and S. R. Quake, *Phys. Rev. Lett.*, 2001, **86**, 4163.
- 29 P. Garstecki, M. J. Fuerstman, H. A. Stone and G. M. Whitesides, *Lab Chip*, 2006, **6**, 437.
- 30 P. Guillot and A. Colin, *Phys. Rev. E*, 2005, **72**, 066301.
- 31 D. R. Link, S. L. Anna, D. A. Weitz and H. A. Stone, *Phys. Rev. Lett.*, 2004, **92**, 054503.
- 32 A. Q. Shen, B. Gleason, G. H. McKinley and H. A. Stone, *Phys. Fluids*, 2002, **14**, 4055–4068.



Looking for that **special** research paper from applied and technological aspects of the chemical sciences?

TRY this free news service:

Chemical Technology

- highlights of newsworthy and significant advances in chemical technology from across RSC journals
- free online access
- updated daily
- free access to the original research paper from every online article
- also available as a free print supplement in selected RSC journals.*

*A separately issued print subscription is also available.

Registered Charity Number: 207890

RSCPublishing

www.rsc.org/chemicaltechnology

22030683